An efficient kinetic modeling in plasmas by using the AWBS transport equation

Authors[a,1]

[a] *Centre Lasers Intenses et Applications, Universite de Bordeaux-CNRS-CEA, UMR 5107, F-33405 Talence, France*

Abstract

Keywords: kinetics; hydrodynamics; nonlocal electron transport; laser-heated plasmas.

*Corresponding author.
E-mail address: milan.holec@u-bordeaux.fr

1. BGK, AWBS, and Fokker-Planck models in local diffusive regime

We can try to find an approximate solution while using the first term of expansion in λ_{ei} and μ as

$$\tilde{f}(z, v, \mu) = f^0(z, v) + f^1(z, v)\lambda_{ei}(v)\mu. \tag{1}$$

1.1. The BGK local diffusive electron transport

$$\mu\left(\frac{\partial f}{\partial z} + \frac{\tilde{E}_z}{v}\frac{\partial f}{\partial v}\right) + \frac{\tilde{E}_z(1-\mu^2)}{v^2}\frac{\partial f}{\partial \mu} = \frac{f - f_M}{\lambda_e} + \frac{1}{2\lambda_{ei}}\frac{\partial}{\partial \mu}(1-\mu^2)\frac{\partial f}{\partial \mu}, \tag{2}$$

$$\begin{aligned} f^0 &= f_M + \frac{1}{v} f^1 \bar{Z}\lambda_{ei}^2, &(3)\\ f^1 &= -\frac{\bar{Z}}{\bar{Z}+1}\left[\frac{\partial f^0}{\partial z} + \frac{\tilde{E}_z}{v}\frac{\partial f^0}{\partial v}\right], &(4)\end{aligned}$$

$$f = f_M - \frac{\bar{Z}}{\bar{Z}+1}\left[\frac{1}{\rho}\frac{\partial \rho}{\partial z} + \left(\frac{v^2}{2v_{th}^2} - \frac{3}{2}\right)\frac{1}{T}\frac{\partial T}{\partial z} - \frac{\tilde{E}_z}{v_{th}^2}\right] f_M \lambda_{ei}\mu,$$

and when holds $\boldsymbol{j} \equiv q_e \int \boldsymbol{v} f \,\mathrm{d}\boldsymbol{v} = \boldsymbol{0} \rightarrow \tilde{\boldsymbol{E}} = v_{th}^2\left(\frac{\nabla\rho}{\rho} + \frac{5}{2}\frac{\nabla T}{T}\right)$, i.e. the electric field $\tilde{E}_z$ obeying the zero current condition leads to

$$f = f_M - \frac{\bar{Z}}{\bar{Z}+1}\left(\frac{v^2}{2v_{th}^2} - 4\right)\frac{1}{T}\frac{\partial T}{\partial z} f_M \lambda_{ei}\mu,$$

1.2. The AWBS diffusive electron transport

$$\begin{aligned}\mu\left(\frac{\partial f}{\partial z} + \frac{\tilde{E}_z}{v}\frac{\partial f}{\partial v}\right) + \frac{\tilde{E}_z(1-\mu^2)}{v^2}\frac{\partial f}{\partial \mu} = \\ \frac{v}{2\lambda_e}\frac{\partial}{\partial v}(f - f_M) + \frac{1}{2}\left(\frac{1}{\lambda_{ei}} + \frac{1}{2\lambda_e}\right)\frac{\partial}{\partial \mu}(1-\mu^2)\frac{\partial f}{\partial \mu}, \quad (5)\end{aligned}$$

$$
\begin{aligned}
\frac{\partial}{\partial v}\left(f^0 - f_M\right) &= \frac{1}{v^2} f^1 \bar{Z}\lambda_{ei}^2, \\
\frac{v}{\bar{Z}\lambda_{ei}}\frac{\partial(f^1\lambda_{ei})}{\partial v} - \frac{\bar{Z}+1}{\bar{Z}} f^1 &= \frac{\partial f^0}{\partial z} + \frac{\tilde{E}_z}{v}\frac{\partial f^0}{\partial v}
\end{aligned}
\tag{6}
$$

$$
\frac{\partial f^1}{\partial v} + \frac{1}{v}(3-\bar{Z})f^1 = \frac{\bar{Z}}{v}\left(\frac{1}{\rho}\frac{\partial \rho}{\partial z} + \left(\frac{v^2}{2v_{th}^2} - \frac{3}{2}\right)\frac{1}{T}\frac{\partial T}{\partial z} - \frac{\tilde{E}_z}{v_{th}^2}\right) f_M. \tag{7}
$$

1.3. The Fokker-Planck diffusive electron transport

$$
\mu\left(\frac{\partial f}{\partial z} + \frac{\tilde{E}_z}{v}\frac{\partial f}{\partial v}\right) + \frac{\tilde{E}_z(1-\mu^2)}{v^2}\frac{\partial f}{\partial \mu} = \\
\frac{\Gamma^{ee}}{v}\left(4\pi f^2 + \frac{\nabla_{\boldsymbol{v}}\nabla_{\boldsymbol{v}} f : \nabla_{\boldsymbol{v}}\nabla_{\boldsymbol{v}} g}{2}\right) + \frac{1}{\lambda_{ei}}\frac{\partial}{\partial \mu}(1-\mu^2)\frac{\partial f}{\partial \mu},
$$

where $g(\boldsymbol{v}) = \int |\boldsymbol{v}-\boldsymbol{v}^*| f(\boldsymbol{v}^*)\,\mathrm{d}\boldsymbol{v}^*$ is the Rosenbluth potential [2]. Since we are interested in the approximate solution in the diffusive regime, it is convenient to use a low anisotropy approximation $\tilde{g} = g^0(f^0) + g^1(f^1)\lambda_{ei}(v)\mu$, which arises from Eq. 45 in [2].

$$
\Gamma^{ee}\left(4\pi \tilde{f}^2 + \frac{\nabla_{\boldsymbol{v}}\nabla_{\boldsymbol{v}} \tilde{f} : \nabla_{\boldsymbol{v}}\nabla_{\boldsymbol{v}} \tilde{g}}{2}\right) = \Gamma^{ee}\left(4\pi {f^0}^2 + \frac{1}{2}\frac{\partial^2 f^0}{\partial v^2}\frac{\partial^2 g^0}{\partial v^2} + \frac{1}{v^2}\frac{\partial f^0}{\partial v}\frac{\partial g^0}{\partial v}\right) \\
+ \mu\Bigg[8\pi f^0 f^1 v^4 - v\left(\frac{\partial f^0}{\partial v} g^1 + \frac{\partial g^0}{\partial v} f^1\right) + \frac{1}{v^2}\left(\frac{\partial f^0}{\partial v}\frac{\partial (g^1 v^4)}{\partial v} + \frac{\partial g^0}{\partial v}\frac{\partial (f^1 v^4)}{\partial v}\right) \\
+ \frac{1}{2}\left(\frac{\partial^2 f^0}{\partial v^2}\frac{\partial^2 (g^1 v^4)}{\partial v^2} + \frac{\partial^2 g^0}{\partial v^2}\frac{\partial^2 (f^1 v^4)}{\partial v^2}\right)\Bigg] + O(\lambda_{ei}^2, \mu^2)
$$

$$
\Gamma^{ee}\left(4\pi {f^0}^2 + \frac{1}{2}\frac{\partial^2 f^0}{\partial v^2}\frac{\partial^2 g^0}{\partial v^2} + \frac{1}{v^2}\frac{\partial f^0}{\partial v}\frac{\partial g^0}{\partial v}\right) = \frac{1}{v^2} f^1 \bar{Z}\lambda_{ei}^2, \tag{8}
$$

$$\frac{1}{2}\left(\frac{\partial^2 f_M}{\partial v^2}\frac{\partial^2(g^1 v^4)}{\partial v^2}+\frac{\partial^2 g_M}{\partial v^2}\frac{\partial^2(f^1 v^4)}{\partial v^2}\right)+\frac{1}{v^2}\left(\frac{\partial f_M}{\partial v}\frac{\partial(g^1 v^4)}{\partial v}+\frac{\partial g_M}{\partial v}\frac{\partial(f^1 v^4)}{\partial v}\right)$$
$$-v\left(\frac{\partial f_M}{\partial v}g^1+\frac{\partial g_M}{\partial v}f^1\right)+8\pi f_M f^1 v^4 - v f^1 = v\frac{\partial f_M}{\partial z}+\tilde{E}_z\frac{\partial f_M}{\partial v}, \quad (9)$$

$$f_1(v,\mu)=\mu\frac{m_e^2}{4\pi e^4 \mathrm{ln}\Lambda}\frac{v_{2th}^4}{\bar{Z}}\left(2d_T(v/v_{2th})+\frac{3}{2}\frac{\gamma_T}{\gamma_E}d_E(v/v_{2th})\right)\frac{f_M(v)}{n_e}\frac{\nabla T}{T}, \quad (10)$$

where $d_T(x)=\bar{Z}D_T(x)/B$ and $d_E(x)=\bar{Z}D_E(x)/A$ are represented by numerical values in TABLE I and TABLE II in [5], respectively.

[2], [3], [4]

1.4. Summary of BGK, AWBS, and Fokker-Planck diffusion

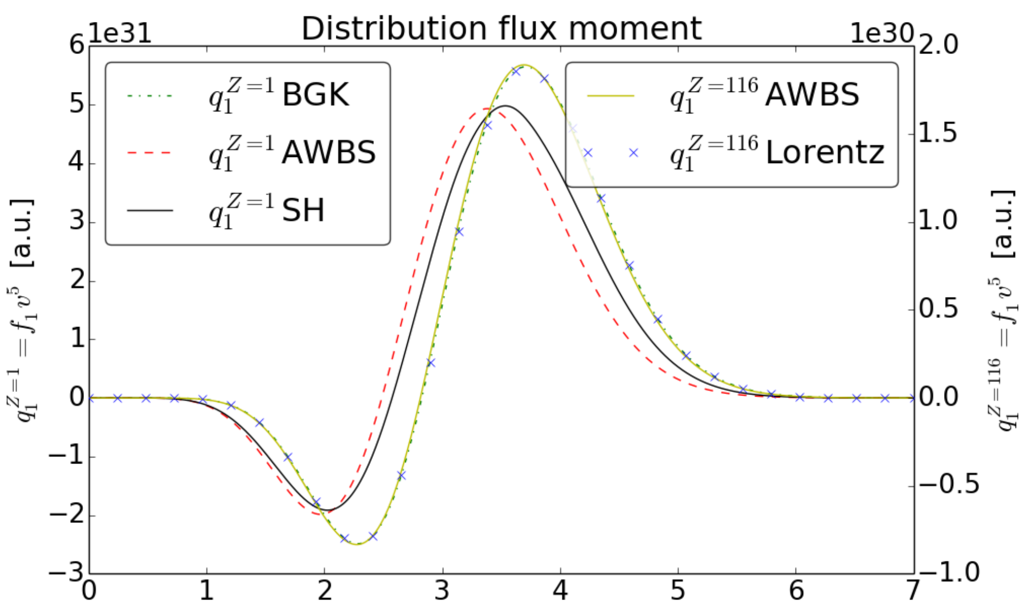

Figure 1: The flux velocity moment of the anisotropic part of the electron distribution function in low $Z=1$ and high $Z=116$ plasmas in diffusive regime.

	$\bar{Z}=1$	$\bar{Z}=2$	$\bar{Z}=4$	$\bar{Z}=16$	$\bar{Z}=116$
$\bar{\Delta}\boldsymbol{q}_{AWBS}$	0.057	0.004	0.038	0.049	0.004

Table 1: Relative error $\bar{\Delta}\boldsymbol{q}_{AWBS} = |\boldsymbol{q}_{AWBS} - \boldsymbol{q}_{SH}|/\boldsymbol{q}_{SH}$ of the AWBS kinetic model equation (**??**) showing the discrepancy (maximum around 5%) with respect to the original solution of the heat flux given by Spitzer and Harm [5].

2. Benchmarking the AWBS nonlocal transport model

2.1. Review of simulation codes

2.2. C7

In order to eliminate the dimensions of the above transport problem the first-two-moment model based on approximation

$$f = \frac{f_0}{4\pi} + \frac{3}{4\pi}\boldsymbol{n}\cdot\boldsymbol{f_1},$$

can be adopted and reads

$$\begin{aligned} v\frac{\nu_e}{2}\frac{\partial}{\partial v}\left(f_0 - 4\pi f_M\right) &= v\nabla\cdot\boldsymbol{f_1} + \tilde{\boldsymbol{E}}\cdot\frac{\partial \boldsymbol{f_1}}{\partial v} + \frac{2}{v}\tilde{\boldsymbol{E}}\cdot\boldsymbol{f_1}, \\ v\frac{\nu_e}{2}\frac{\partial \boldsymbol{f_1}}{\partial v} - \left(\nu_{ei} + \frac{\nu_e}{2}\right)\boldsymbol{f_1} &= \frac{v}{3}\nabla f_0 + \frac{\tilde{\boldsymbol{E}}}{3}\frac{\partial f_0}{\partial v}, \end{aligned}$$

$$\boldsymbol{q}_c \equiv q_e\int_v\left(\frac{\nu_e v^2}{\nu_{ei}+\frac{\nu_e}{2}}\frac{\partial \boldsymbol{f_1}}{\partial v} - \frac{v^2}{3\left(\nu_{ei}+\frac{\nu_e}{2}\right)}\nabla f_0 - \frac{v}{3\left(\nu_{ei}+\frac{\nu_e}{2}\right)}\frac{\partial f_0}{\partial v}\tilde{\boldsymbol{E}}\right)v^2\,\mathrm{d}v = 0,$$

2.2.1. Nonlocal electric field treatment

$$\begin{aligned} &\left(v\frac{\nu_e}{2} - \frac{2\tilde{E}_z^2}{3v\nu_e}\right)\frac{\partial f_{1_z}}{\partial v} = \\ &\qquad \frac{2\tilde{E}_z}{3\nu_e}\frac{\partial f_{1_z}}{\partial z} + \frac{4\pi\tilde{E}_z}{3}\frac{\partial f_M}{\partial v} + \frac{v}{3}\frac{\partial f_0}{\partial z} + \left(\frac{4\tilde{E}_z^2}{3v^2\nu_e} + \left(\nu_{ei} + \frac{\nu_e}{2}\right)\right)f_{1_z}, \end{aligned}$$

Kn	10^{-3}	5×10^{-3}	10^{-2}	5×10^{-2}	10^{-1}
$v_{lim}^{Z=2}/v_{th}$	14.8	6.8	5.0	2.8	2.6
$v_{lim}^{Z=10}/v_{th}$	6.7	3.4	2.6	1.6	1.3

Table 2: $\sqrt{3}v\frac{\nu_e}{2} > \tilde{E}_z$.

$$
\begin{aligned}
|\tilde{\boldsymbol{E}}_{red}| &= v\frac{\nu_e}{2}, \\
\nu_{ei}^E &= \frac{|\tilde{\boldsymbol{E}}| - |\tilde{\boldsymbol{E}}_{red}|}{v},
\end{aligned}
$$

where $\omega_{red} = |\tilde{\boldsymbol{E}}_{red}|/|\tilde{\boldsymbol{E}}|$.

P1 approximation equivalent

$$
f = \frac{4\pi f_M + \delta f_0}{4\pi} + \frac{3}{4\pi}\boldsymbol{n} \cdot \boldsymbol{f_1}. \tag{11}
$$

where the moment model reads

$$
\begin{aligned}
v\frac{\nu_e}{2}\frac{\partial \delta f_0}{\partial v} &= v\nabla \cdot \boldsymbol{f_1} + \tilde{\boldsymbol{E}} \cdot \left(\omega_{red}\frac{\partial \boldsymbol{f_1}}{\partial v} + \frac{2}{v}\boldsymbol{f_1}\right), \\
v\frac{\nu_e}{2}\frac{\partial \boldsymbol{f_1}}{\partial v} &= \left(\nu_{ei} + \nu_{ei}^E + \frac{\nu_e}{2}\right)\boldsymbol{f_1} + \frac{v}{3}\nabla\left(4\pi f_M + \delta f_0\right) \\
&\quad + \frac{\tilde{\boldsymbol{E}}}{3}\left(4\pi\frac{\partial f_M}{\partial v} + \omega_{red}\frac{\partial \delta f_0}{\partial v}\right),
\end{aligned}
$$

$$
\tilde{\boldsymbol{E}} = \frac{\int_v \left(\frac{\frac{\nu_e}{2}v^2}{\nu_{ei}+\nu_{ei}^E+\frac{\nu_e}{2}}\frac{\partial \boldsymbol{f_1}}{\partial v} - \frac{v^2}{3\left(\nu_{ei}+\nu_{ei}^E+\frac{\nu_e}{2}\right)}\nabla\left(4\pi f_M + \delta f_0\right)\right) v^2\,\mathrm{d}v}{\int_v \frac{v}{3\left(\nu_{ei}+\nu_{ei}^E+\frac{\nu_e}{2}\right)}\left(4\pi\frac{\partial f_M}{\partial v} + \omega_{red}\frac{\partial \delta f_0}{\partial v}\right) v^2\,\mathrm{d}v},
$$

2.3. Aladin

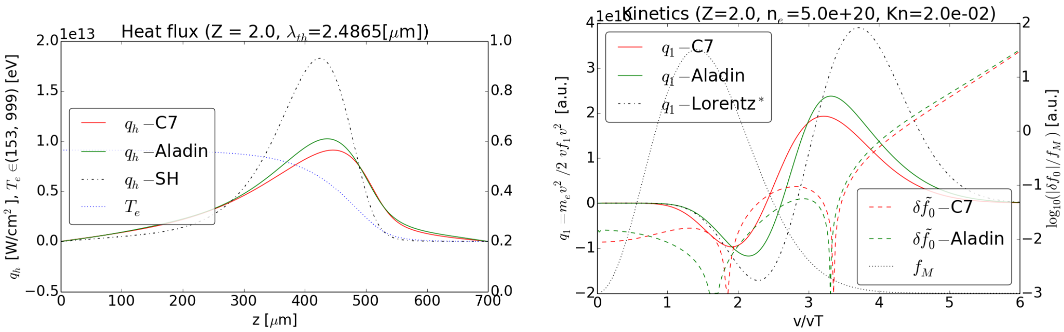

Figure 2: Snapshot 12 ps. Left: correct steady solution of heat flux. Right: correct comparison to kinetic profiles at point 442 μm by Aladin.

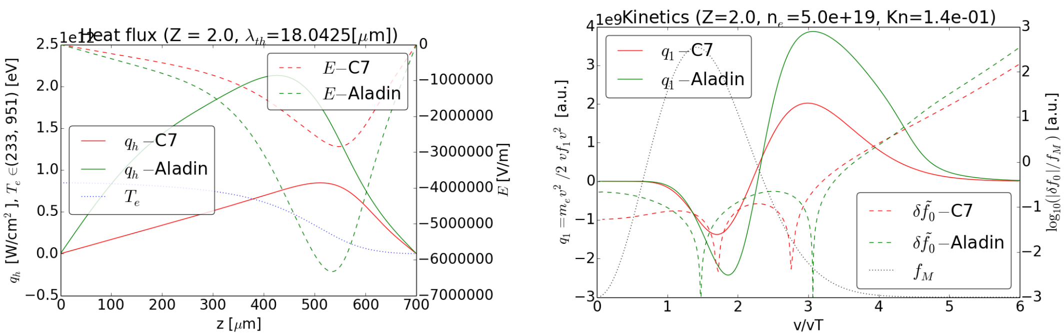

Figure 3: Snapshot 12 ps. Left: correct steady solution of heat flux. Right: correct comparison to kinetic profiles at point 480 μm by Aladin.

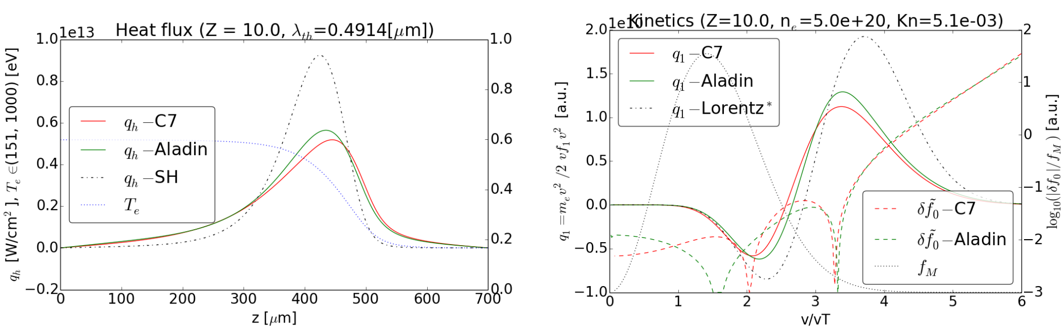

Figure 4: Snapshot 12 ps. Left: correct steady solution of heat flux. Right: correct comparison to kinetic profiles at point 442 μm by Aladin.

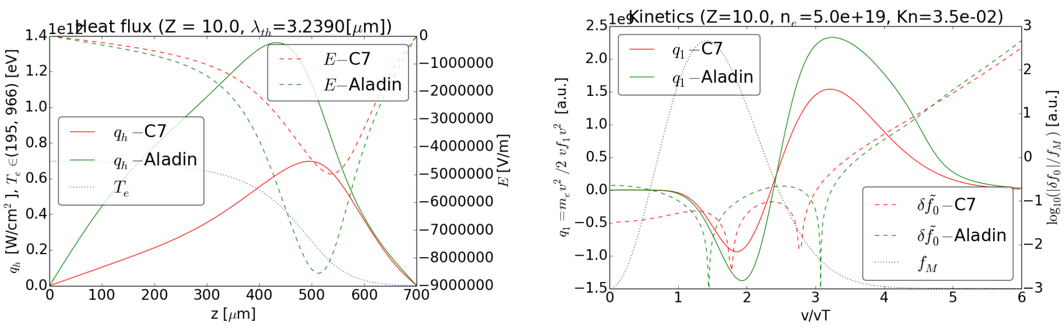

Figure 5: Snapshot 12 ps. Left: correct steady solution of heat flux. Right: correct comparison to kinetic profiles at point 480 μm by Aladin.

2.4. Impact

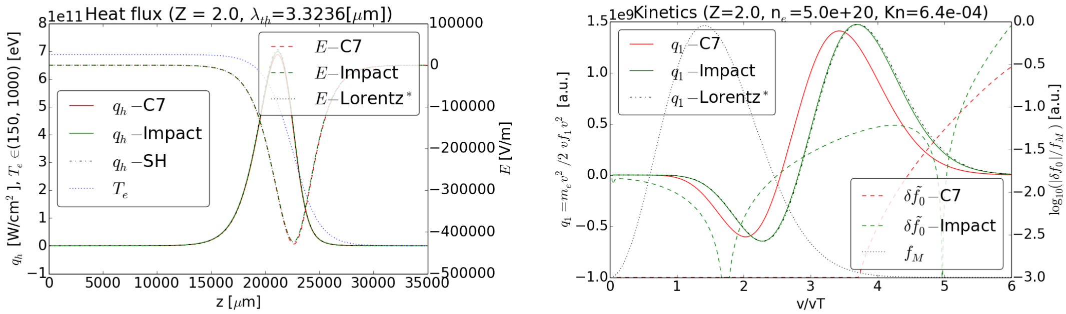

Figure 6: Impact diffusive case 1.

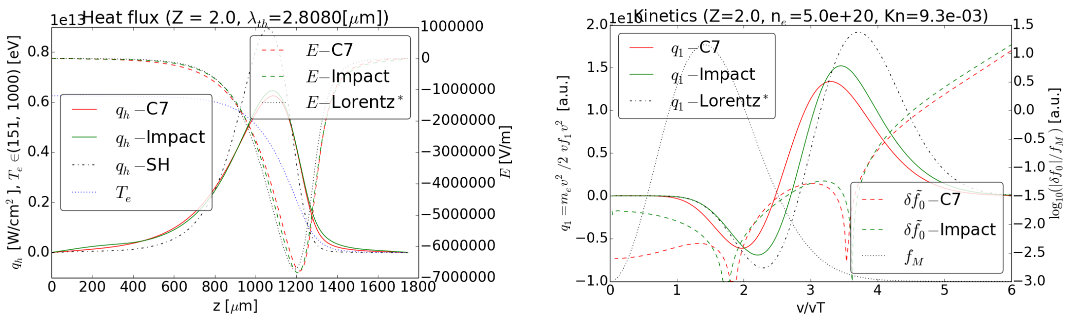

Figure 7: Impact case 2.

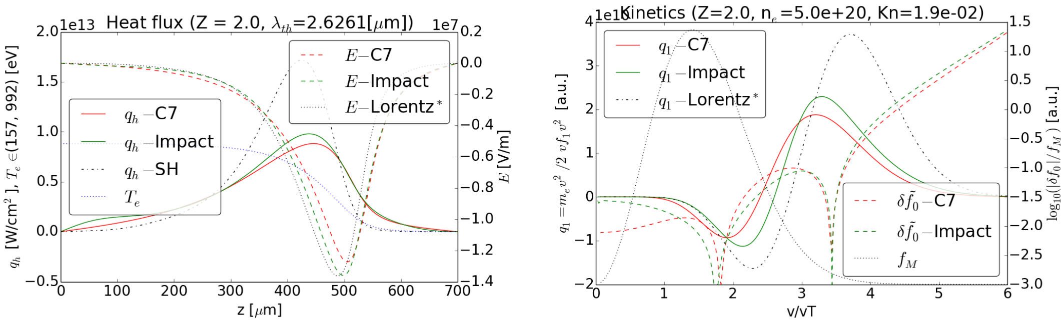

Figure 8: Snapshot 12 ps. Left: correct steady solution of heat flux. Right: correct comparison to kinetic profiles at point 437 μm by Impact.

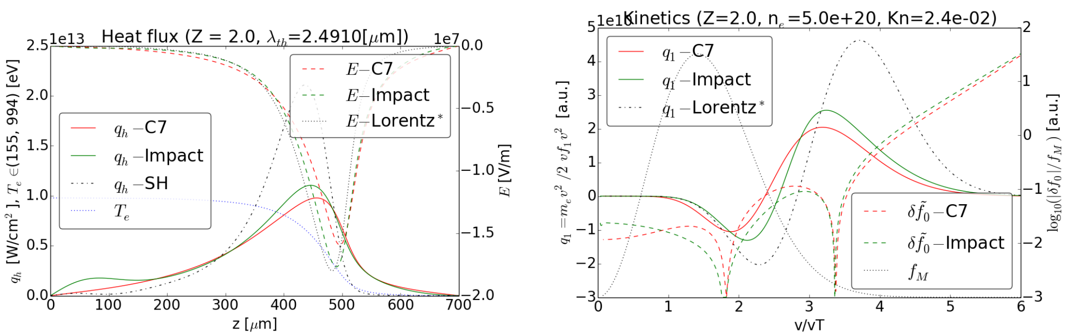

Figure 9: Impact case 4.

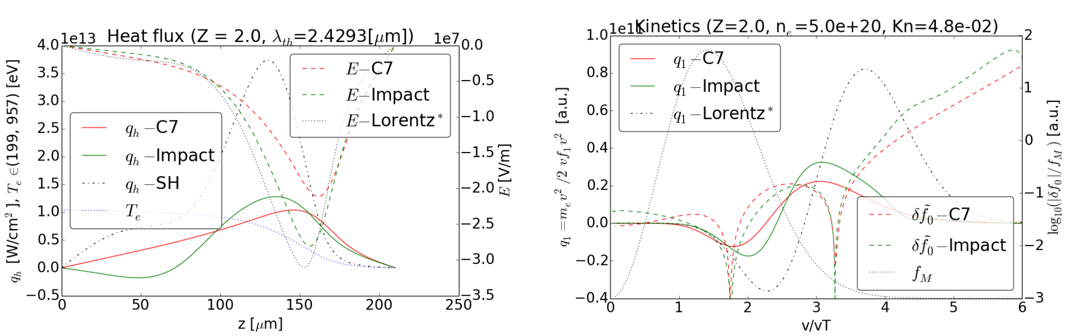

Figure 10: Impact case 5.

2.5. Calder

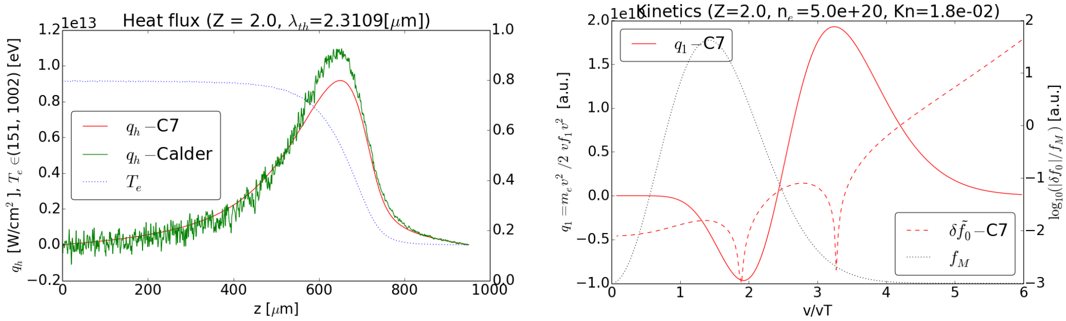

Figure 11: Snapshot 11 ps. Left: correct steady solution of heat flux. Right: Kinetic profiles at point of maximum flux by C7. Kinetics profiles by CALDER should be added.

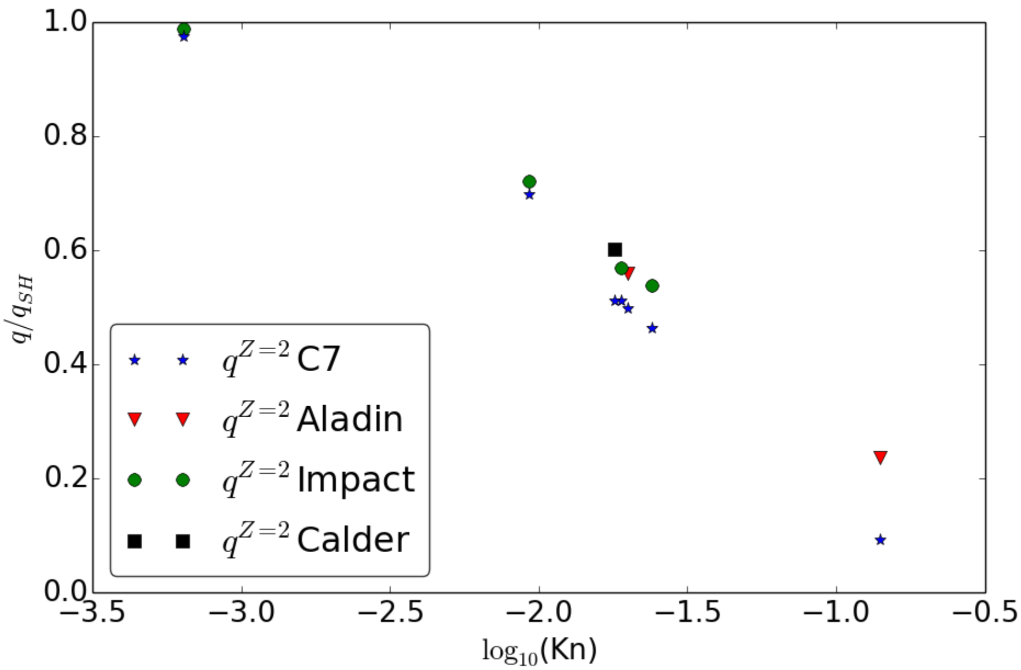

Figure 12: Simulation results for the case $Z = 2$ computed by C7/Aladin/Impact/Calder. Every point corresponds to the maximum heat flux in a "tanh" temperature simulation, which can be characterized by Kn. The range of $\log_{10}(\mathrm{Kn}) \in (-0.5, -3.5)$ can be expressed as equivalent to the electron density approximate range $\mathrm{n}_e \in (5e19, 3.5e22)$ of the 50 μm slope tanh case.

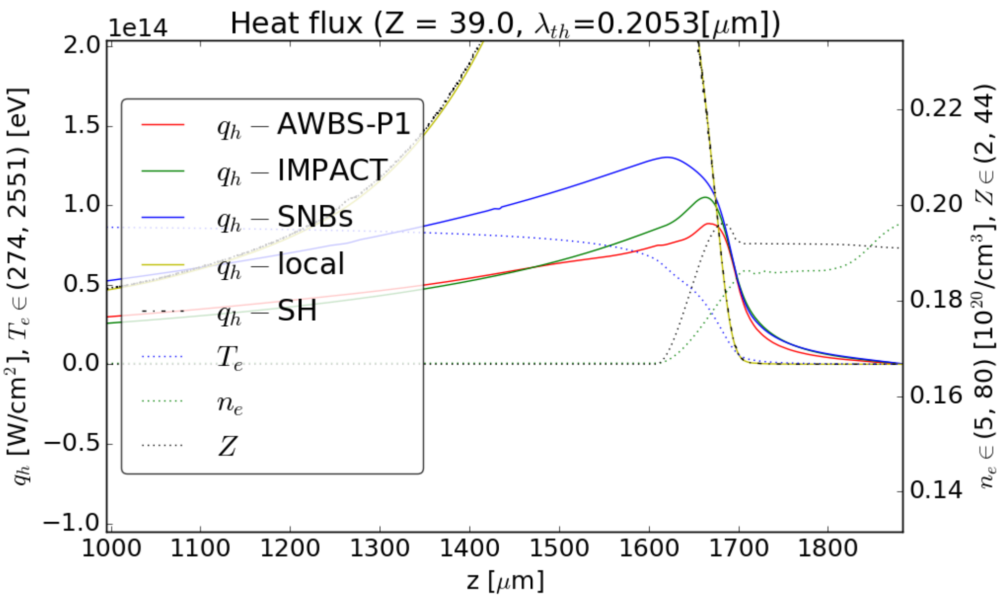

Heat flux (Z = 39.0, λ_{th}=0.2053[μm])
1e14
2.0
1.5
1.0
0.5
0.0
−0.5
−1.0
q_h [W/cm^2], $T_e \in$ (274, 2551) [eV]
$q_h -$ AWBS-P1
$q_h -$ IMPACT
$q_h -$ SNBs
$q_h -$ local
$q_h -$ SH
T_e
n_e
Z
0.22
0.20
0.18
0.16
0.14
$n_e \in$ (5, 80) [10^{20}/cm^3], $Z \in$ (2, 44)
1000
1100
1200
1300
1400
1500
1600
1700
1800
z [μm]

Figure 13:

3. Conclusions

[1] Nathaniel J. Fisch. Theory of current drive in plasmas. Rev. Mod. Phys., 59(1):175234, Jan 1987.

[2] Marshall N. Rosenbluth, William M. MacDonald, and David L. Judd. Fokker-planck equation for an inverse-square force. Phys. Rev., 107(1):16, Jul 1957.

[3] Longmire, Conrad L. : Elementary Plasma Physics. Intersci. Pub., 1963.

[4] I.P. Shkarofsky, T.W. Johnston, T.W. Bachynski, The Particle Kinetics of Plasmas, Addison-Wesley, Reading, MA, 1966.

[5] SH 1953.